Surface Atomic Arrangement Dependence of Electrochemical CO2 Reduction on Gold: Online Electrochemical Mass Spectrometric Study on Low-Index Au(hkl) Surfaces

doi: 10.1021/acscatal.8b04852

Surface Atomic Arrangement Dependence of Electrochemical CO_2 Reduction on Gold: Online Electrochemical Mass Spectrometric Study on Low-Index Au(*hkl*) Surfaces

Naoto Todoroki, Hiroki Tei, Hiroto Tsurumaki, Taku Miyakawa, Tatsuhiko Inoue and Toshimasa Wadayama*

Graduate School of Environmental Studies, Tohoku University, Sendai 980-8579, Japan

Corresponding Author

*; corresponding author

E-mail: n-todoroki@material.tohoku.ac.jp

ABSTRACT

We evaluated the electrochemical reduction reaction of CO_2 (ECR) on low-index Au single crystal surfaces (Au(111), (100), and (110); Au(*hkl*)) and discussed the surface-atomic-arrangement-dependence of Au on the ECR. Online-electrochemical mass spectrometry (OLEMS) results revealed that the onset potential of the quadrupole mass spectrometer (Q-mass) ion signal for the reduction product carbon monoxide (CO; m/z =28) is ca. 0.3 V lower on the Au(110) surface than on the Au(111) and (100) surfaces. Furthermore, the Au(110) surface showed a superior selectivity for CO generation in the potential region of −0.4V to −1.4V vs. reversible hydrogen electrode (RHE); the relative, OLEMS-corrected ECR partial current density for generated CO at −0.76 V was ca. 20-fold higher compared with the Au(100) and (111) surfaces. The Tafel slope of Au(110) at the onset potential region (around −0.4V) was much smaller than that of the Au(111) and (100) surfaces, suggesting that Au(110) shows the fastest ECR kinetics among the low-index Au surfaces. The results obtained in this study reveal that the ECR efficiency as well as the selectivity for CO generation on Au electrode surfaces can be dominated by the surface atomic arrangements and that relative Faradaic selectivity evaluation by OLEMS is helpful for discussion of the ECR process.

Keywords; Electrochemical CO_2 reduction, gold electrode, carbon dioxide, carbon monoxide, single crystal surfaces, online electrochemical mass spectrometry

TOC GRAPHIC

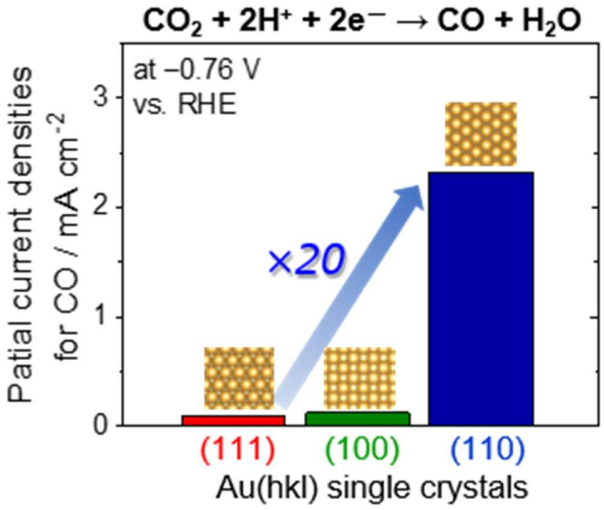
CO2 + 2H+ + 2e− → CO + H2O
at −0.76 V
vs. RHE
Patial current densities
for CO / mA cm-2
0
1
2
3
×20
(111)
(100)
(110)
Au(hkl) single crystals

MAIN TEXT

The electrochemical reduction reaction of CO_2 (ECR) is one of the most effective approaches to converting the green-house gas molecule of CO_2 to valuable carbon-based chemical substances, such as carbon monoxide (CO), formic acid (HCOOH), or C1-C2 carbohydrates[1-7]. It is well known that the reduction products of the ECR are strongly dependent on the electrode materials used[8-9], e.g., Au, Ag, or Zn, and these alloys mainly generate CO with high energy efficiencies[10-15]. However, further improvements in both the efficiency and selectivity of CO generation are required for the industrialization of the ECR.

Electrode-catalytic reactions on metals and alloys are strongly influenced by the surface atomic arrangements[16-19]. As for the ECR, pioneering works by Hori and coworkers are well-known for examining the low- and high-index surfaces of Cu, Pd, Ag, and Pt single crystals[20-24]. Furthermore, a new insight was recently reported[25-27] for intermediate species and elementary steps of the ECR on Cu single crystal surfaces. However, as for Au single crystal surfaces, while DFT calculations for the adsorption energies of the reaction intermediates have been conducted and reported[11, 28-29], no experimental studies aimed at clarifying the dependence on the Au surface atomic arrangements have been reported yet. In addition to the surface atomic arrangement dependences of the electrode materials, the electrochemical efficiency and selectivity of the ECR depend strongly on the applied potentials[8]. To date, the ECR efficiency and selectivity are mainly discussed in relation to the polarization curve and objective product analysis at a static applied potential by using gas-chromatography[3]. Because the ECRs for the objective- and by-products proceed simultaneously on the same electrode surface, it is necessary to clarify the contribution of each product to the total ECR current to discuss the selectivity and activity. Therefore, *in-situ* analysis of individual ECR products (CO, H_2, etc.) on the electrode surface while sweeping the

electrochemical potential is indispensable for a discussion of the effect of the surface atomic arrangement of the Au electrodes. This will provide essential information for the development of practical Au electrode-catalysts for ECR.

In this study, we evaluated the electrochemical efficiency and selectivity of the ECR on ultra-high vacuum (UHV; ~10^{-8} Pa) cleaned low-index single crystal surfaces of Au, i.e., Au(111), Au(100), and Au(111), by using polarization curve measurements while simultaneously performing online electrochemical mass spectrometric (OLEMS) measurements. The onset potentials of the polarization curves during potential sweeps in the negative direction depend upon the surface atomic arrangements of Au. The OLEMS results clearly showed that, over the potential range of −0.4 to −1.4 V, the relative Faradaic selectivity for the reduction product of CO is highest on the Au(110) surface. On the basis of the polarization curves and OLEMS results, we conclude that superior electrochemical efficiency and selectivity for the ECR to CO can be obtained on Au(110), in comparison with the Au(100) and (111) surfaces.

Au(111), (100), and (110) disk electrodes (φ = 12 mm, t = 1 mm) were used as working electrodes. Hereafter, we simply denote the sample electrodes as "Au(*hkl*)". The electrode surfaces were cleaned by repeated cycles of Ar^+ ion sputtering and annealing at 1073 K in UHV. The UHV-cleaned Au(*hkl*) electrodes were transferred to the electrochemical setup without air exposure by using a sample transfer vessel[30] and were set in the electrochemical cell (Figure 1) in an N_2-purged glove box to avoid any contamination of the electrode surface. Surface characterization of the UHV-cleaned Au(*hkl*) samples was conducted using a scanning tunneling microscope (STM) in UHV and cyclic voltammetry measurements in 0.1 M $HClO_4$ at a room temperature. Detailed results are described in the Supporting Information.

Figure 1 shows a schematic drawing of the home-made OLEMS system used in this study. The ECR on the Au(*hkl*) electrodes was conducted in CO_2-saturated 0.1 M $KHCO_3$. The home-made H-type two compartment cell with a Pt-wire counter electrode, a Ag/AgCl(3 M) reference electrode and the Au(*hkl*) working electrode (WE) was used for the ECR measurements[31]. The geometrical surface area of the WE exposed to the electrolyte was confined to be 0.635 cm^2 by an O-ring. With reference to the paper by Wonders et al.[32], porous Teflon (pore size = 10 μm) was inserted into a gas sampling tip to prevent direct introduction of the solution into the quadrupole mass spectrometer (Q-mass; SRS RGA100) equipped vacuum system. The distance between the tip and the Au(*hkl*) electrode surface was kept constant at several tens of micrometers. Retardation of the ECR-product detection by the Q-mass was estimated to be ca. 15 s caused by the rather low conductance of the vacuum line connected to the EC cell. Considering the retardation time, the electrode potentials of the OLEMS spectra were compensated to compare the ECR currents on the corresponding polarization curves. Onset potentials both for the EC polarization curves and Q-mass ion signals are defined as applied potentials corresponding to 1 % intensity of the maximum EC current density or Q-mass ion signals.

Polarization curves (a) and corresponding OLEMS spectra (b) of the Au(*hkl*) electrodes recorded in CO_2-saturated 0.1 M $KHCO_3$ are presented in Figure 2. The ECR current densities over the potential regions below −0.4 V increased in the order of Au(111) < Au(100) < Au(110). A close inspection of the onset potential region (ca. −0.2 V; inset in Figure 2 (a)) reveals that only the Au(110) surface showed a small feature at −0.23 V (marked by *). This faint feature probably corresponds to the adsorption of intermediates, e.g., COOH or CO, on the metal electrodes[33], suggesting that such reaction intermediates tend to stabilize on the Au(110) surface. One might notice that the onset potential of ECR current is lowest for the Au(111) surface (inset of (a)),

though the overall ECR current for the Au(110) surface is highest. As shown in the corresponding OLEMS results for the reduction product CO (*m/z* = 28; middle panel in (b)), the Au(110) surface showed the largest Q-mass ion signal intensity and a much higher onset potential in comparison with the Au(111) and Au(100) surfaces. In contrast, Q-mass ion signal intensity for H_2 (m/z = 2) was the lowest for the Au(110), except for the onset potential region where the Au(111) is almost the same to the Au(110). Although CH_4 (*m/z* = 15) was detected above a noise-level below the potential region of ca. −0.6 V, the intensities of *m/z* = 15 were very weak relative to those for H_2 and CO (bottom panel of (b)) for all the Au(*hkl*). As for formate ($HCOO^-$), which is known to be a very small amount product of the ECR on the Au electrode [34], no Q-mass ion signal due to a fragment of formate (*m/z* = 45; $HCOO^-$) was detected for all the Au(*hkl*) surfaces in this OLEMS condition (Figure S3 in the Supporting Information). Table 1 summarizes the onset potentials of the Au(*hkl*) electrodes for the ECR currents (on the polarization curves (a)) and Q-mass ion signals (OLEMS (b)) of H_2 (*m/z* = 2) and CO (*m/z* = 28). While the onset potentials of the ECR currents and that of the CO Q-mass ion signals for both the Au(111) and (100) surfaces were the almost same, the onset potential for Au(110) was ca. 0.3 V higher than that of the Au(111) and (100) surfaces. Furthermore, for Au(100), although the CO Q-mass ion signal showed similar behavior on Au(111) up to −1.0 V, the signal of H_2 was much weaker than on Au(111). The results suggest that the Au(100) surface shows higher selectivity for the generation of CO in comparison to Au(111). In other words, the ECR by-product of H_2 is correlated with the lowest onset potential of ECR current for the Au(111) surface (Figure 2(a) inset).

In this study, the relative Faradaic selectivity for the objective ECR gaseous product (RFS_x) was calculated by using the following equation (1)[35],

$$RFS_x = \frac{2I_x}{2I_{H_2} + 2I_{CO} + 8I_{CH_4}} \times 100\ (\%) \quad (1)$$

where x is the objective ECR product (H_2, CO, and CH_4 in this study) and I_x is the corresponding Q-mass ion signal intensity (Figure 2 (b)). The RFS_x values of CO (RFS_{CO}) vs. electrode potentials are presented in Figure 3. Because the Q-mass intensities below −0.4 V were rather weak and fluctuated, the RFS_x values are plotted for the potential region from −0.4 V to −1.4 V. The results indicate that Au(110) showed a much higher RFS_{CO} than the Au(100) and (111) surfaces over the potential region; the difference is particularly noticeable at low potential regions around −0.6 V, suggesting that the Au(110) surface can generate CO with high selectivity even at a low potential, i.e., the low ECR current density region.

Partial current densities for each reaction product were calculated by multiplying the corresponding RFS values of H_2 and CO by the current densities of the polarization curves (Figure 2(a)); the results are summarized in Figure 4 (a). The partial current density of CH_4 is excluded because of its faint Q-mass signal intensity (Figure 2(b)). It can be clearly seen that the partial current density for H_2 is comparably independent of the surface atomic arrangement of Au, though close inspection reveals that the Au(111) surface showed the lowest onset potential for the ECR current (Figure 2(a) inset). In contrast, the value of the partial current density for the generation of CO is remarkable for Au(110), even over the estimated potential regions. By reference to the previous study[36], we used the partial current densities at −0.76 V to determine the electrochemical generation efficiency for CO; the results are plotted in Figure 4(b). As can clearly be seen, the Au(110) surface showed ca. 20 times higher partial current density than the Au(111) and (100) surfaces, clearly indicating the highest selectivity to CO.

Tafel plots of partial current densities for CO (Figure 4 (c)) estimated from the polarization curves and corresponding OLEMS results support the strong dependence of the ECR activation energy on the surface atomic arrangements of Au. The Tafel slope for Au(110) at the onset potential region (−0.4 ~ −0.5 V) was estimated to be 117 mV/dec. This value was much smaller than that for Au(111) (208 mV/dec) and Au(100) (181 mV/dec) at the onset regions (−0.6 ~ −0.7 V) and, furthermore, is also smaller than the reported value of 140 mV/dec for a polycrystalline Au film that was evaluated in a 0.1 M $NaHCO_3$ solution[37]. Liu et al. reported the reaction kinetics for the ECR on low-index Au(*hkl*) surfaces based on density functional theory (DFT) calculations and deduced that the Gibbs free-energy change (ΔG) for the first uphill reaction step, i.e., $CO_2 + H^+ + e^- + * \rightarrow COOH*$ (* is a surface adsorption site), is the smallest for the Au(110) surface[28]. Therefore, the difference in estimated Tafel slopes (Figure 4(c)) probably reflects the fact that the first reaction step is faster for the Au(110) surface than for the Au(111), Au(100), and polycrystalline Au surfaces[37]. Such structural dependence of the Tafel slopes has been reported for nanostructured Cu and Au catalysts[10, 38].

Published papers for the ECR on the nanostructured Au catalysts, e.g., monodispersed nanoparticles (NPs)[39], [40], nanowires[41], and oxide-derived Au[10] discussed the surface structural effects. For example, Zhu et al. investigated the ECR properties of the size-confined Au nanoparticles with diameters of 4 to 8 nm[39]. Their DFT results show that COOH* intermediate adsorbates become more stabilized on Au(211) surface having low-coordinated step (edge) sites (coordination number (CN) = 7) in comparison to Au(111) (CN = 9), while CO adsorption energy of the two surfaces are almost same. As for the corner-sites (CN = 6), the CO adsorption energy is too large. In accordance with the results, they deduced that 8 nm NPs, which has appropriate number of edge sites ((CN) = 7), showed the highest CO selectivity; maximum faradaic selectivity

value for CO of the 8 nm NPs is over 90 %. The selectivity value of 90 % is higher than the estimated value of 79 % for the UHV-cleaned Au(110) (CN = 7; Figure 3). Therefore, the estimated CO selectivity might also be influenced by minor surface sites of the Au(*hkl*) surfaces, e.g., steps, kinks and atomic defects.

Also, OLEMS investigations for oxidation/reduction reactions (redox) of the ECR-related adsorbates and/or product molecules, e.g., formate, formaldehyde and CO should provide deeper insights to the ECR mechanisms, because such the molecules should also correlate with the element reaction steps of the ECR. In fact, as for the CO oxidation reaction, Koper and coworkers clarified the difference in CO adsorption sites and the adsorption energy depending on the catalyst surface atomic arrangements by combined analysis of electrochemistry, spectroscopy and DFT calculations[42-43]. OLEMS analysis for the stepped single crystal surfaces and for the ECR-related molecules should provide crucial information for developing highly efficient Au-based CO_2 electroreduction nanostructured catalysts.

Conclusions

We first showed the dependence of the ECR on the surface atomic arrangement of the Au(*hkl*) electrodes from the electrochemical polarization curves and OLEMS measurements in CO_2-saturated 0.1 M $KHCO_3$. The onset potential for the generation of CO on the Au(110) surface as evaluated from the Q-mass ion signal intensities was ca. −0.4 V; the over potential was ca. 0.3 V lower than on Au(111) and (100). Furthermore, the Au(110) surface showed higher selectivity for CO generation in the applied potential range from −0.4 to −1.4 V and the partial ECR current density for CO at −0.76 V was ca. 20 times higher than on the Au(100) and (111) surfaces. The

results demonstrate that the OLEMS measurements are indispensable for discussion of the ECR process, particularly in terms of the dependence of the ECR efficiency, selectivity, and reaction kinetics on the surface atomic arrangements. Future OLEMS study for the high-index single crystal surfaces of Au and for the redox of by-product molecules should provide deeper insights to the CO_2 reduction mechanisms. Also, Surface engineering to ensure precise control of the low-coordination surface sites of nano-structured catalysts, such as edges and/or corners, is essential for achieving superior electrochemical efficiency of CO_2 conversion to CO on Au and Au-based alloy electrodes.

ASSOCIATED CONTENT

Supporting Information

The supporting information is available free of charge on the ACS Publications website at DOI: The surface structural observations of the Au(*hkl*) samples by UHV-STM, the cyclic voltammograms recorded in N_2-purged 0.1 M $HClO_4$, and OLEMS results for formate.

AUTHOR INFORMATION

E-mail: n-todoroki@material.tohoku.ac.jp

Notes

The authors declare no competing financial interest.

ACKNOWLEDGMENT

This study was partly supported by a Grant-in-Aid for scientific research (A) from the

Japan Society for the Promotion of Science (T.W.)

REFERENCES

(1) Raciti, D.; Wang, C. Recent Advances in CO_2 Reduction Electrocatalysis on Copper. *ACS Energy Lett.* 2018, 3, 1545-1556.
(2) Vickers, J. W.; Alfonso, D.; Kauffman, D. R. Electrochemical Carbon Dioxide Reduction at Nanostructured Gold, Copper, and Alloy Materials. *Energy Technol.* 2017, 5, 775-795.
(3) Lu, Q.; Jiao, F. Electrochemical CO_2 Reduction: Electrocatalyst, Reaction Mechanism, and Process Engineering. *Nano Energy* 2016, 29, 439-456.
(4) Qiao, J.; Liu, Y.; Hong, F.; Zhang, J. A Review of Catalysts for the Electroreduction of Carbon Dioxide to Produce Low-Carbon Fuels. *Chem. Soc. Rev.* 2014, 43, 631-675.
(5) Devin, T. W.; Paul, J. A. K. Prospects of CO_2 utilization Via Direct Heterogeneous Electrochemical Reduction. *J. Phys. Chem. Lett.* 2010, 1, 3451-3458.
(6) Gattrell, M.; Gupta, N.; Co, A. Electrochemical Reduction of CO_2 to Hydrocarbons to Store Renewable Electrical Energy and Upgrade Biogas. *Energy Convers. Manag.* 2007, 48, 1255-1265.
(7) Gattrell, M.; Gupta, N.; Co, A. A Review of the Aqueous Electrochemical Reduction of CO_2 to Hydrocarbons at Copper. *J. Electroanal. Chem.* 2006, 594, 1-19.
(8) Hori, Y., Electrochemical CO_2 Reduction on Metal Electrodes. In *Modern Aspects of Electrochemistry*, Vayenas, C. G.; White, R. E.; Gamboa-Aldeco, M. E., Eds. Springer New York: New York, NY, 2008; pp 89-189.
(9) Kuhl, K. P.; Hatsukade, T.; Cave, E. R.; Abram, D. N.; Kibsgaard, J.; Jaramillo, T. F. Electrocatalytic Conversion of Carbon Dioxide to Methane and Methanol on Transition Metal Surfaces. *J. Am. Chem. Soc.* 2014, 136, 14107-14113.
(10) Chen, Y.; Li, C. W.; Kanan, M. W. Aqueous CO_2 Reduction at Very Low Overpotential on Oxide-Derived Au Nanoparticles. *J. Am. Chem. Soc.* 2012, 134, 19969-19972.
(11) Back, S.; Yeom, M. S.; Jung, Y. Active Sites of Au and Ag Nanoparticle Catalysts for CO_2 Electroreduction to CO. *ACS Catal.* 2015, 5, 5089-5096.
(12) Rosen, J.; Hutchings, G. S.; Lu, Q.; Forest, R. V.; Moore, A.; Jiao, F. Electrodeposited Zn Dendrites with Enhanced Co Selectivity for Electrocatalytic CO_2 Reduction. *ACS Catal.* 2015, 5, 4586-4591.
(13) Ham, Y. S.; Choe, S.; Kim, M. J.; Lim, T.; Kim, S.-K.; Kim, J. J. Electrodeposited Ag Catalysts for the Electrochemical Reduction of CO_2 to CO. *Appl. Catal., B* 2017, 208, 35-43.

(14) Sun, K.; Wu, L.; Qin, W.; Zhou, J.; Hu, Y.; Jiang, Z.; Shen, B.; Wang, Z. Enhanced Electrochemical Reduction of CO_2 to CO on Ag Electrocatalysts with Increased Unoccupied Density of States. *J. Mater. Chem. A* 2016, 4, 12616-12623.
(15) Moreno-García, P.; Schlegel, N.; Zanetti, A.; Cedeño López, A.; Gálvez-Vázquez, M. d. J.; Dutta, A.; Rahaman, M.; Broekmann, P. Selective Electrochemical Reduction of CO_2 to Co on Zn-Based Foams Produced by Cu^{2+} and Template-Assisted Electrodeposition. *ACS Appl. Mater.* 2018, 10, 31355-31365.
(16) Stamenkovic, V. R.; Fowler, B.; Mun, B. S.; Wang, G.; Ross, P. N.; Lucas, C. A.; Markovic, N. M. Improved Oxygen Reduction Activity on Pt3ni(111) Via Increased Surface Site Availability. *Science* 2007, 315, 493-497.
(17) Yamada, Y.; Miyamoto, K.; Hayashi, T.; Iijima, Y.; Todoroki, N.; Wadayama, T. Oxygen Reduction Reaction Activities for Pt-Enriched Co/Pt(111), Co/Pt(100), and Co/Pt(110) Model Catalyst Surfaces Prepared by Molecular Beam Epitaxy. *Surf. Sci.* 2013, 607, 54-60.
(18) Markovica, N. M.; Sarraf, S. T.; Gasteiger, H. A.; Ross, P. N. Hydrogen Electrochemistry on Platinum Low-Index Single-Crystal Surfaces in Alkaline Solution. *J. Chem. Soc. Frad. Trans.* 1996, 92, 3719-3725.
(19) Lee, S. W.; Chen, S.; Suntivich, J.; Sasaki, K.; Adzic, R. R.; Shao-Horn, Y. Role of Surface Steps of Pt Nanoparticles on the Electrochemical Activity for Oxygen Reduction. *J. Phys. Chem. Lett.* 2010, 1, 1316-1320.
(20) Takahashi, I.; Koga, O.; Hoshi, N.; Hori, Y. Electrochemical Reduction of CO_2 at Copper Single Crystal Cu(S)-[N(111)×(111)] and Cu(S)-[N(110)×(100)] Electrodes. *J. Electroanal. Chem.* 2002, 533, 135-143.
(21) Hoshi, N.; Kagaya, K.; Hori, Y. Voltammograms of the Single-Crystal Electrodes of Palladium in Aqueous Sulfuric Acid Electrolyte: Pd(S)-[N(111)×(111)] and Pd(S)-[N(100)×(111)]. *J. Electroanal. Chem.* 2000, 485, 55-60.
(22) Hoshi, N.; Kawatani, S.; Kudo, M.; Hori, Y. Significant Enhancement of the Electrochemical Reduction of CO_2 at the Kink Sites on Pt(S)-[N(110)×(100)] and Pt(S)-[N(100)×(110)]. *J. Electroanal. Chem.* 1999, 467, 67-73.
(23) Hoshi, N.; Kato, M.; Hori, Y. Electrochemical Reduction of CO_2 on Single Crystal Electrodes of Silver Ag(111), Ag(100) and Ag(110). *J. Electroanal. Chem.* 1997, 440, 283-286.
(24) Hoshi, N.; Suzuki, T.; Hori, Y. CO_2 Reduction on Pt(S) -[N(111) × (111)] Single Crystal Electrodes Affected by the Adsorption of Sulfuric Acid Anion. *J. Electroanal. Chem.* 1996, 416, 61-65.
(25) Schouten, K. J. P.; Qin, Z.; Gallent, E. P.; Koper, M. T. M. Two Pathways for the Formation of Ethylene in Co Reduction on Single-Crystal Copper Electrodes. *J. Am. Chem. Soc.* 2012, 134, 9864-9867.
(26) Pérez-Gallent, E.; Marcandalli, G.; Figueiredo, M. C.; Calle-Vallejo, F.; Koper, M. T. M. Structure- and Potential-Dependent Cation Effects on Co Reduction at Copper Single-Crystal Electrodes. *J. Am. Chem. Soc.* 2017, 139, 16412-16419.
(27) Huang, Y.; Handoko, A. D.; Hirunsit, P.; Yeo, B. S. Electrochemical Reduction of CO_2 Using Copper Single-Crystal Surfaces: Effects of CO* Coverage on the Selective Formation of Ethylene. *ACS Catal.* 2017, 7, 1749-1756.
(28) Liu, M.; Pang, Y.; Zhang, B.; De Luna, P.; Voznyy, O.; Xu, J.; Zheng, X.; Dinh, C. T.; Fan, F.; Cao, C.; de Arquer, F. P. G.; Safaei, T. S.; Mepham, A.; Klinkova, A.; Kumacheva, E.; Filleter, T.; Sinton, D.; Kelley, S. O.; Sargent, E. H. Enhanced Electrocatalytic CO_2 Reduction Via Field-Induced Reagent Concentration. *Nature* 2016, 537, 382-386.

(29) Shi, C.; Hansen, H. A.; Lausche, A. C.; Norskov, J. K. Trends in Electrochemical CO_2 Reduction Activity for Open and Close-Packed Metal Surfaces. *Phys. Chem. Chem. Phys.* 2014, 16, 4720-4727.
(30) Wadayama, T.; Todoroki, N.; Yamada, Y.; Sugawara, T.; Miyamoto, K.; Iijama, Y. Oxygen Reduction Reaction Activities of Ni/Pt(111) Model Catalysts Fabricated by Molecular Beam Epitaxy. *Electrochem. Commun.* 2010, 12, 1112-1115.
(31) Todoroki, N.; Yokota, N.; Nakahata, S.; Nakamura, H.; Wadayama, T. Electrochemical Reduction of CO_2 on Ni- and Pt-Epitaxially Grown Cu(111) Surfaces. *Electrocatalysis* 2016, 7, 97-103.
(32) Wonders, A. H.; Housmans, T. H. M.; Rosca, V.; Koper, M. T. M. On-Line Mass Spectrometry System for Measurements at Single-Crystal Electrodes in Hanging Meniscus Configuration. *J. Appl. Electrochem.* 2006, 36, 1215-1221.
(33) Hori, Y.; Murata, A.; Takahashi, R. Formation of Hydrocarbons in the Electrochemical Reduction of Carbon Dioxide at a Copper Electrode in Aqueous Solution. *J. Chem. Soc. Farad. Trans. 1* 1989, 85, 2309.
(34) Hori, Y.; Wakebe, H.; Tsukamoto, T.; Koga, O. Electrocatalytic Process of Co Selectivity in Electrochemical Reduction of CO_2 at Metal Electrodes in Aqueous Media. *Electrochim. Acta* 1994, 39, 1833-1839.
(35) Reske, R.; Duca, M.; Oezaslan, M.; Schouten, K. J. P.; Koper, M. T. M.; Strasser, P. Controlling Catalytic Selectivities During CO_2 Electroreduction on Thin Cu Metal Overlayers. *J. Phys. Chem. Lett.* 2013, 4, 2410-2413.
(36) Kim, D.; Resasco, J.; Yu, Y.; Asiri, A. M.; Yang, P. Synergistic Geometric and Electronic Effects for Electrochemical Reduction of Carbon Dioxide Using Gold–Copper Bimetallic Nanoparticles. *Nat. Commun.* 2014, 5, 4948.
(37) Wuttig, A.; Yaguchi, M.; Motobayashi, K.; Osawa, M.; Surendranath, Y. Inhibited Proton Transfer Enhances Au-Catalyzed CO_2 to Fuels Selectivity. *Proc. Natl. Acad. Sci.* 2016, 113, E4585-E4593.
(38) Kas, R.; Kortlever, R.; Milbrat, A.; Koper, M. T. M.; Mul, G.; Baltrusaitis, J. Electrochemical CO_2 Reduction on Cu_2O-Derived Copper Nanoparticles: Controlling the Catalytic Selectivity of Hydrocarbons. *Phys. Chem. Chem. Phys.* 2014, 16, 12194-12201.
(39) Zhu, W.; Michalsky, R.; Metin, Ö.; Lv, H.; Guo, S.; Wright, C. J.; Sun, X.; Peterson, A. A.; Sun, S. Monodisperse Au Nanoparticles for Selective Electrocatalytic Reduction of CO_2 to CO. *J. Am. Chem. Soc.* 2013, 135, 16833-16836.
(40) Mistry, H.; Reske, R.; Zeng, Z.; Zhao, Z.-J.; Greeley, J.; Strasser, P.; Cuenya, B. R. Exceptional Size-Dependent Activity Enhancement in the Electroreduction of CO_2 over Au Nanoparticles. *J. Am. Chem. Soc.* 2014, 136, 16473-16476.
(41) Zhu, W.; Zhang, Y.-J.; Zhang, H.; Lv, H.; Li, Q.; Michalsky, R.; Peterson, A. A.; Sun, S. Active and Selective Conversion of CO_2 to CO on Ultrathin Au Nanowires. *J. Am. Chem. Soc.* 2014, 136, 16132-16135.
(42) Shubina, T. E.; Hartnig, C.; Koper, M. T. M. Density Functional Theory Study of the Oxidation of CO by OH on Au(110) and Pt(111) Surfaces. *Phys. Chem. Chem. Phys.* 2004, 6, 4215-4221.
(43) Rodriguez, P.; Garcia-Araez, N.; Koverga, A.; Frank, S.; Koper, M. T. M. CO Electroxidation on Gold in Alkaline Media: A Combined Electrochemical, Spectroscopic, and Dft Study. *Langmuir* 2010, 26, 12425-12432.

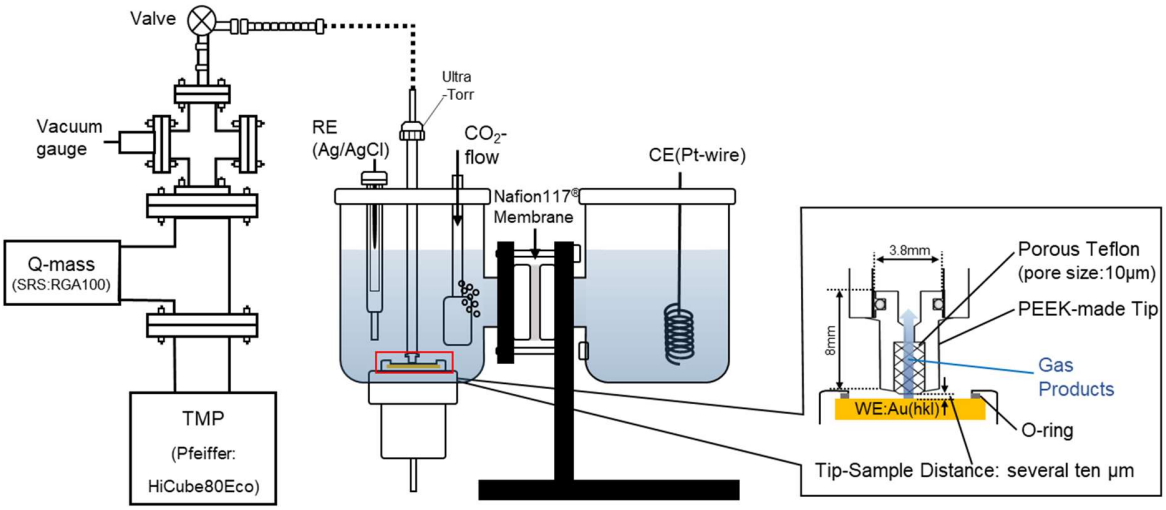

Figure 1. Schematic of the home-made OLEMS system used in this study

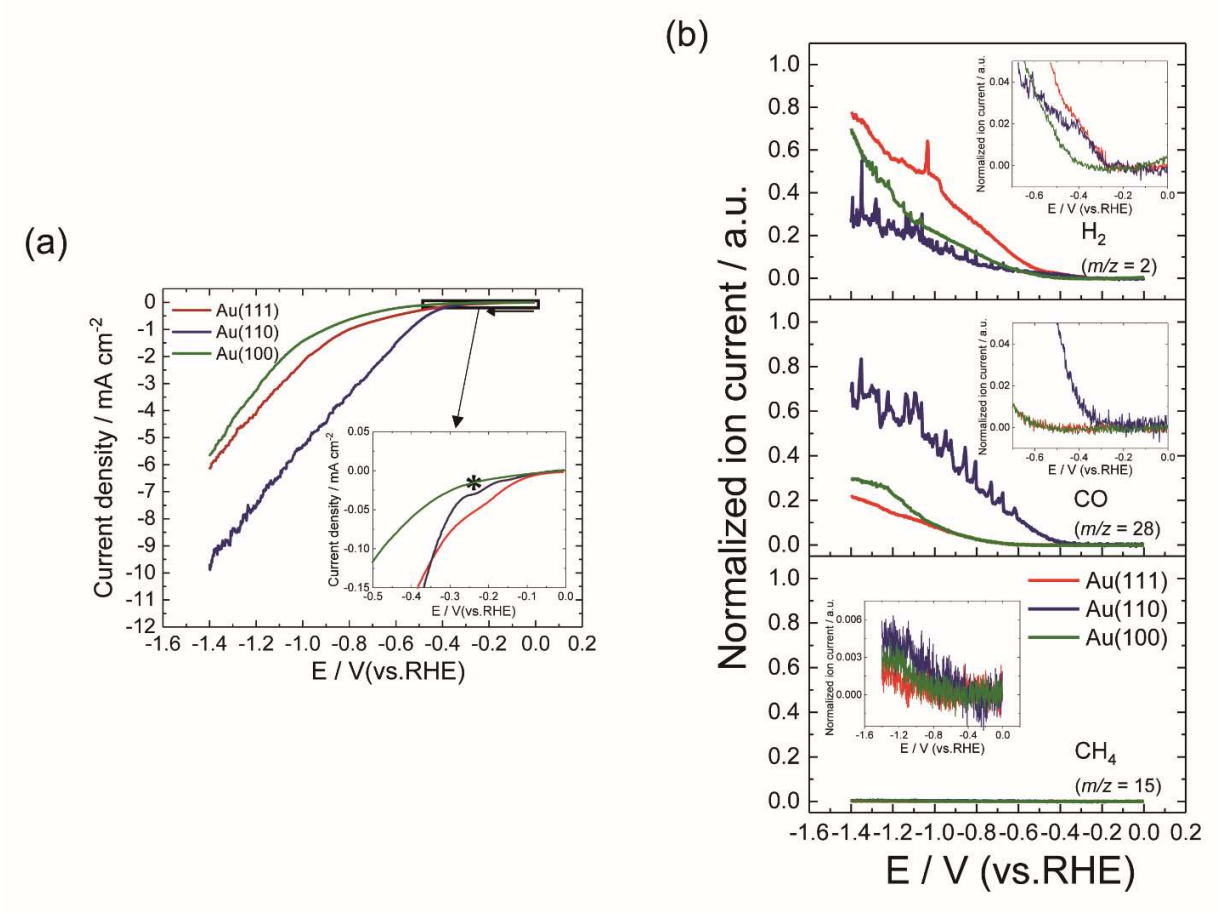

Figure 2. (a) Polarization curves of Au(*hkl*) recorded in a CO_2-saturated 0.1 M $KHCO_3$ solution at 1 mV/s. (b) Normalized Q-mass ion currents for hydrogen, carbon monoxide, and methane probed by OLEMS with dependence of the applied cathodic potential. Insets are magnifications of onset potential regions.

Table 1. Onset potentials estimated from polarization curves and OLEMS ion currents for H_2 and CO.

	Onset Potentials (V vs. RHE)		
	Polarization Curves (ECR Current)	Q-mass ion signal (OLEMS)	
		H_2 (*m/z* = 2)	CO (*m/z* = 28)
Au(111)	-0.33	-0.31	-0.66
Au(110)	-0.34	-0.34	-0.37
Au(100)	-0.48	-0.48	-0.66

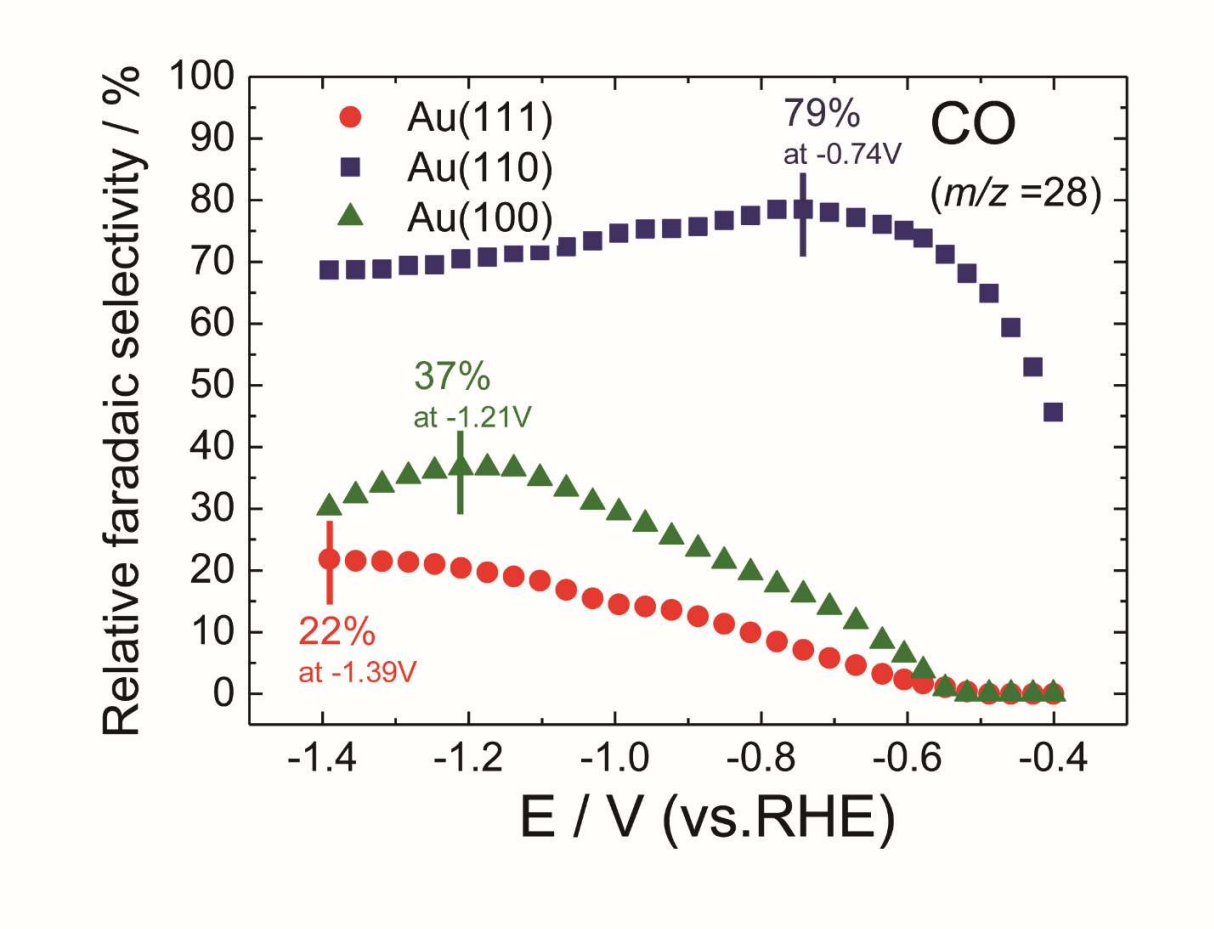

Figure 3. Relative Faradaic selectivity for CO (RFS_{CO}) on the Au(*hkl*) surfaces.

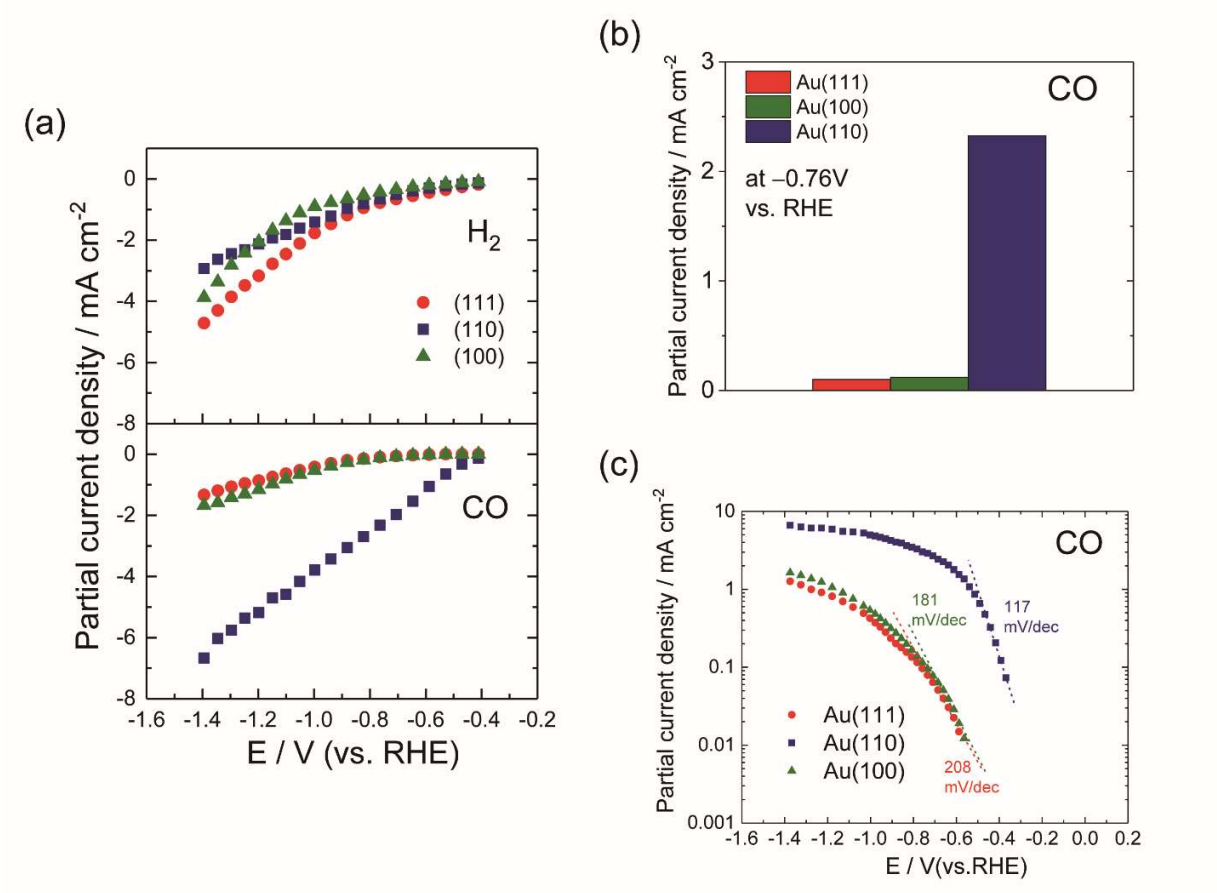

Figure 4. (a) Partial current densities for H_2 and CO on the Au(*hkl*) surfaces vs. applied potentials. (b) The partial current densities at −0.76 V vs. RHE for Au(*hkl*). (c) Tafel plots for CO partial current densities.